# Dynamics of ethylene photodissociation from rovibrational and translational energy distributions of H2 products

Evan F. Cromwell, Albert Stolow, Marcus J. J. Vrakking, and Yuan T. Lee

Citation: The Journal of Chemical Physics **97**, 4029 (1992); doi: 10.1063/1.462942
View online: http://dx.doi.org/10.1063/1.462942
View Table of Contents: http://scitation.aip.org/content/aip/journal/jcp/97/6?ver=pdfcov
Published by the AIP Publishing



# Dynamics of ethylene photodissociation from rovibrational and translational energy distributions of $H_2$ products

Evan F. Cromwell, Albert Stolow, Marcus J. J. Vrakking, and Yuan T. Lee
*Chemical Sciences Division, Lawrence Berkeley Laboratory and Department of Chemistry, University of California, Berkeley, California 94720*

(Received 6 May 1992; accepted 2 June 1992)

The dynamics of $H_2$ elimination from ethylene was studied via a pump and probe technique utilizing an ultrahigh resolution vacuum ultraviolet laser system. $H_2$ product internal and translational energy distributions were obtained for the photodissociation at 193 nm. The distribution of energy in $H_2$ product from the dissociation of (1,1)-dideuteroethylene is also presented. Two separate $H_2$ elimination channels are inferred: a 1,1 elimination producing the vinylidene radical and a 1,2 elimination producing the acetylene molecule. Differences between the vibrational, rotational, and translational energy distributions for these two channels are discussed and correlations between product internal and translational energy are presented. A comparison with *ab initio* calculations of the transition state configurations for these processes is made. We suggest that the $H_2$ elimination process may be nonstatistical in nature. The D atom elimination from $C_2D_4$ was examined and kinetic energy distribution for this product measured.

## I. INTRODUCTION

The study of the unimolecular decomposition of ethylene ($C_2H_4$) has been of great interest to the scientific community for more than 30 years. The importance of this molecule comes not only from its worth to industry as a precursor to many widely used materials, but also from its value as a test of *ab initio* computation for a six-atom system.

Early experiments determined the major unimolecular reaction pathways for $C_2H_4$ to be elimination of H [reaction (1)] and elimination of $H_2$ [reaction (2)]; both forming acetylene

$$C_2H_4 \rightarrow C_2H_2 + 2H, \tag{1}$$

$$C_2H_4 \rightarrow C_2H_2 + H_2. \tag{2}$$

These experiments were typically performed in a "bulb" using a variety of excitation sources including radiolysis,[1,2] mercury sensitization,[3] flash photolysis,[4] and discharge lamps.[5–9] It was found that the above two channels are roughly equiprobable for 193 nm dissociation. However, a number of important questions remained regarding the structures of the intermediates and the electronic potential energy surfaces involved in the different reactive processes.

The next important steps came with the detection of two radical intermediates in the ethylene reaction scheme: the vinyl ($CH_2CH\cdot$) and vinylidene ($CH_2C$:) species. These species had both been predicted theoretically, but it was not known whether their lifetimes would be long enough to permit detection. The presence of $CH_2CH\cdot$ was confirmed initially by detection of products which could only result from the presence of $CH_2CH\cdot$ in the reactive process.[4,10] The existence of the biradical, $CH_2C$:, was not confirmed until much later when appropriate laser light sources had been developed in order to detect it by spectroscopic means.[11–13] The vinylidene formed was found to be in an electronically excited triplet state ($^3B_2$), instead of its ground singlet state, $A(^1B_{1u})$. The temporal evolution of the triplet species suggested that it was not produced by the primary reactive process: this has been recently reinterpreted as being due to secondary photodissociation of the nascent vinyl radical.[14]

The mechanism of H-atom elimination from $C_2H_4$ has been well characterized.[14–16] Following excitation with a vacuum ultraviolet (vuv) photon, $C_2H_4^*$ can internally convert to the ground electronic state after which H-atom elimination occurs via simple bond rupture leading to the formation of energized $CH_2CH\cdot$. The excited vinyl radical can then either subsequently decay into acetylene plus another H atom (provided the initial excitation energy is high enough) or react with other species that might be present. The mechanism for the elimination of molecular hydrogen from $C_2H_4$, however, is not as well determined. The initially proposed reaction mechanism provided for two pathways: a 1,1 hydrogen elimination (1,1*E*) from one of the carbons leaving behind $CH_2C$: [reaction (3)], or a 1,2 hydrogen elimination (1,2*E*) across the carbon–carbon double bond forming acetylene [reaction (4)]

$$H_2C{=}CH_2 \rightarrow H_2C{=}C{:} + H_2, \tag{3}$$

$$H_2C{=}CH_2 \rightarrow HC{\equiv}CH + H_2. \tag{4}$$

From studies of deuterated species the ratio for $H_2$ production between these two pathways, reactions (3) to (4), was determined to be approximately 3:2.[1,6,14] The total amount of energy available to the $H_2$ formed from reaction (3) is only 50–60 kcal/mol because of the high $\Delta H_f^0$ of vinylidene ($\approx$100 kcal/mol).[17] The energy available to $H_2$ from reaction (4) is approximately twice as large at 106.3 kcal/mol. (The $\Delta H_f^0$'s for all pertinent species in the dissociation of $C_2H_4$ are given in Fig. 1.)

The spectroscopy and excited states of ethylene have been reviewed in some detail.[18] The planar ground state is labeled $N(^1\Sigma_g^+)$, while the first excited singlet state is des-

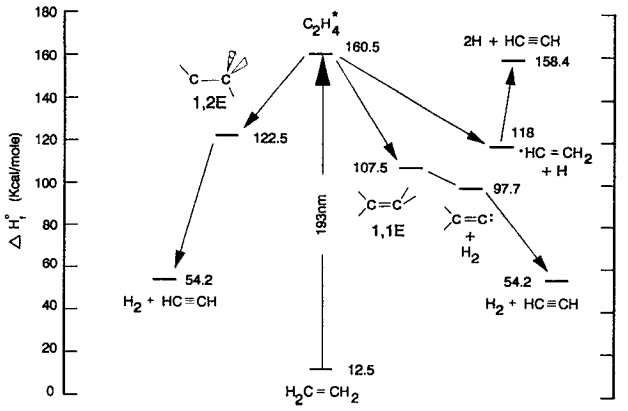


FIG. 1. Standard heat of formations of the pertinent species involved in the dissociation of $C_2H_4$ at 193 nm. Energies are given in kcal/mol. Two transition structures, labeled 1,1*E* and 1,2*E*, are shown. Their geometries and energetics are based upon the work of Yoshimine (Ref. 23).

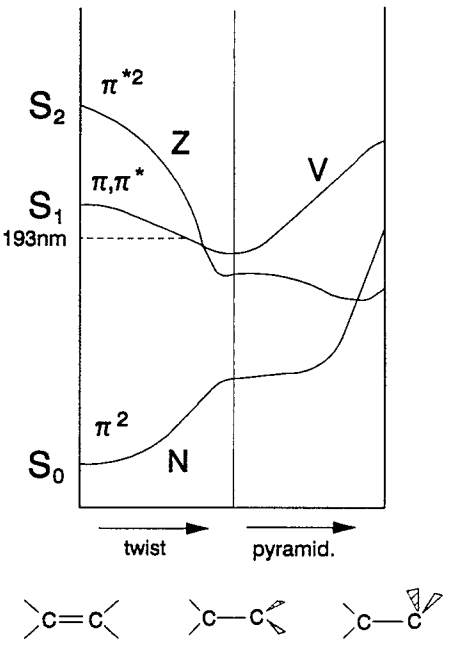


FIG. 2. State correlation diagram showing curve crossing in ethylene, based upon the work of Yoshimine (Ref. 23). As the methylene groups twist, the initially prepared *V* state intersects the *Z* state which, in turn, intersects the ground state (*N*) upon pyramidalization. The transition, *V* to *Z* to *N*, is an internal conversion process and is thought to be very fast. We expect that the photochemistry of ethylene should be described as occuring on the singlet ground state potential energy surface.

ignated $V(^1\Sigma_u^+)$. The broad, diffuse $V \leftarrow N$ band system extends from 215 nm into the vuv with the intensity rapidly rising towards shorter wavelengths. It is considered to be the prototypical $\pi^* \leftarrow \pi$ transition. The first Rydberg transitions appear at 174.4 nm. The *V* state of ethylene is twisted; it has a potential energy minimum for the methylene groups in a perpendicular configuration. It is capable, however, of free internal rotation for 193 nm (148 kcal/mol) excitation. A third state predicted to be involved in the photochemistry of ethylene is the $Z(^1A_1)$ state which has a $\pi^{*2}$ character. In this state the two methylene groups are pyramidalized[15] and in that configuration the *Z* state becomes the lowest lying electronic state.

A considerable amount of theoretical work has been done relating to the problem of ethylene photochemistry.[19–22] In Fig. 2, we show a schematic correlation diagram[23] for the relevant electronic states in ethylene. The excited *V* state of ethylene correlates directly, with small barrier, to the ground singlet state of vinylidene plus $H_2$. However, the *V* state correlates with neither the singlet ground state of acetylene nor the singlet ground state of the vinyl radical, but does correlate with the singlet ground state of ethylidene ($CHCH_3$). Therefore, the 1,2*E* of $H_2$ and the H atom elimination should be viewed as occurring on the ground state surface. Ethylidene, initially postulated as an intermediate, has been shown to be unstable with respect to rearrangement. Recently, *ab initio* calculations, by Yoshimine, of some transition structures involved in the elimination of molecular hydrogen from $C_2H_4$ have been communicated to the authors.[23] These results will be discussed later.

The experiments reported in this paper examine the rotational, vibrational, and translational energy distributions of the nascent $H_2$ product from the photodissociation of $C_2H_4$ at 193 nm. The D-atom elimination channel from $C_2D_4$ was also examined for information about the translational energy of the D product. In order to distinguish between the two $H_2$ elimination channels further experiments with deuterated ethylene were carried out. $H_2$ product from the dissociation of 1,1 dideuteroethylene (1,1-$d_2$) was analyzed in the same manner, allowing for a direct comparison between the products from the 1,1*E* and 1,2*E* channels in ethylene. The data presented below are consistent with two distinct channels for formation of $H_2$ each of which distributes differently the available energy amongst product degrees of freedom.

## II. EXPERIMENT

The molecular beam apparatus and the vuv–xuv laser system used in these experiments have been described previously.[24,25] A pump and probe technique was used to photolyze ethylene molecules in a molecular beam and then to probe the nasawnt $H_2$ products after a short time delay. The pump and probe beams were collinear and counterpropagating. The probe laser ionized the product $H_2$ molecules via (1+1) resonance enhanced multiphoton ionization (REMPI).[26,27] The resultant ions were detected by time-of-flight mass spectrometry using a Daly-type ion detector.

The probe laser system employed pulsed amplification of the output from a ring dye laser (Coherent 699-29). Computer controlled scanning of the ring laser provided the tuning ability of the probe laser. This high energy, near-transform limited pulse of visible light was then frequency doubled, forming ultraviolet (uv) light, and subsequently tripled or sum-frequency mixed in a pulsed rare gas jet to produce vuv or extreme ultraviolet (xuv) radia-

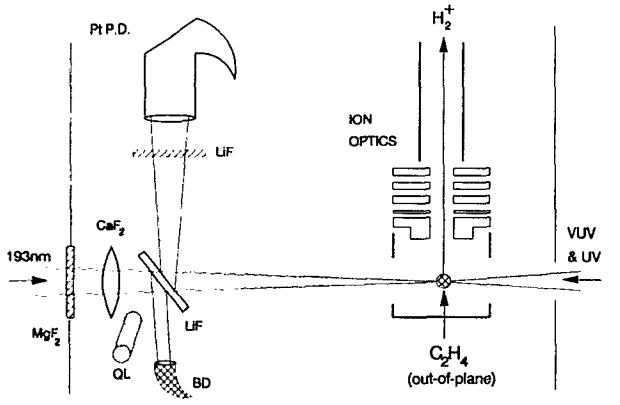


FIG. 3. Schematic of the interaction area in the main chamber for the dissociation of $C_2H_4$ experiment. The substrates of the various optical components are indicated. Pt p.d.=platinum photodiode, QL=quartz heat lamp, and BD=Wood's Horn beam dump for 193 nm beam reflection.

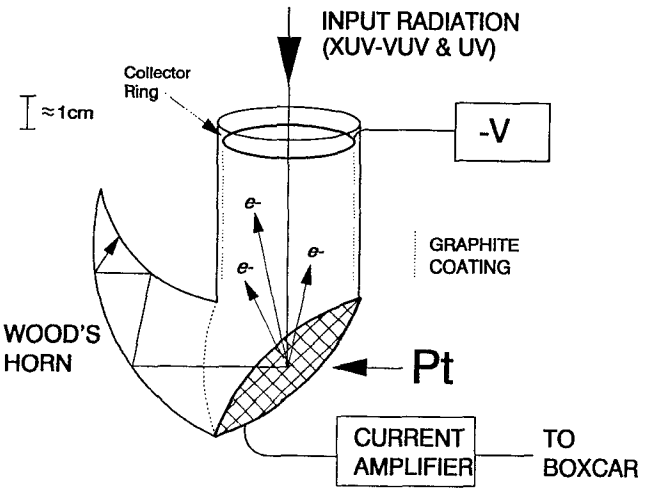


FIG. 4. Schematic of the platinum photodiode used to measure vuv and xuv radiation intensity. The main body (shown roughly to scale) is constructed of glass and the Pt is held in place with wire. $-V$=Low voltage power supply, CR=electron collector ring.

tion. A schematic view of the setup of the laser and molecular beams in the main reaction chamber is shown in Fig. 3.

A 193 nm ArF excimer laser (Lambda-Physik EMG-103-MSC) was used as the photolysis source. The temporal pulse width of the laser output was 20 ns and the pulse to pulse jitter was ±1 ns. An unstable resonator laser cavity was utilized in order to provide a uniform photolysis beam intensity in the interaction region and to maximize the brightness (Watt/steradian) of the laser beam. An 8 mm diameter section of the beam containing up to 10 mJ of energy was selected and sent into the main chamber where it was then focused to a 2 mm spot size with a 50 cm $CaF_2$ lens. The excimer laser output was randomly polarized.

The beam steering optics were dichroic high reflecting, 45° mirrors coated for 193 nm (Acton Research Inc.). The input window to the main chamber was a 25 mm diameter, 3 mm thick $MgF_2$ laser grade window which was rotated occasionally to avoid the attenuation of the laser due to the formation of color centers. All optics inside the main chamber were kept hot with a quartz heat lamp in order to minimize burn spot formation due to photolysis of adsorbed diffusion pump oil.

The 699–29 laser used in these experiments is extremely sensitive to external sources of vibration which can cause unstable operation. Since the excimer laser was on an optical table in contract with the 699–29 laser, it was necessary to vibrationally isolate the excimer laser head (which contained a mechanically "noisy" gas processing unit) from the table. Electrical noise from the discharge in the laser chamber did not adversely affect the 699–29 laser.

It is essential, when determining product state distributions, to accurately normalize signals with respect to drift and fluctuation in output of both the pump and probe lasers. Therefore, careful measurement of the vuv–xuv and excimer laser pulse energies was required. A pyroelectric detector (Molectron J3-09) measured the 193 nm pulse energy, as transmitted through one of the high reflectance mirrors. A sandblasted fused silica window, used as a diffuser, was placed in front of the pyroelectric device as an attenuation source.

For xuv–vuv normalization, a platinum photodiode (p.d.) was used to monitor the probe laser intensity after the interaction region. The use of this type of system has been noted by Tonkyn and White.[28] A slightly different design was developed in this laboratory, a schematic drawing of which is shown in Fig. 4. The vuv light impinges upon a disk of Pt metal ejecting electrons (by the photoelectric effect) which are collected by a biased metal ring. The charge lost from the Pt disk is then amplified via a charge sensitive preamplifier. The uv light is discriminated against by two methods. The high work function of the Pt metal (around 5.65 eV) prohibits electrons from being ejected by single uv photons. However, in practice there was a fair amount of background electrons from the uv, perhaps due to multiphoton effects. In order to further reduce this background, a negative (retarding) bias was applied to the collector ring. Since electrons generated by uv light will generally be of much lower kinetic energy than those generated by vuv photons, they will not be able to overcome as high a potential difference. Application of a −0.5 to −2.0 V bias was enough to reduce the uv background signal. This bias was adjusted to maximize the ratio between vuv and uv signal. Under typical conditions, the ratio between the vuv and uv signals was 8:1.

A 25 mm diameter, 2 mm thick LiF window was used to reflect a fraction of the probe beam and send it directly in to the Pt photodiode (see Fig. 2). This photodiode provided excellent discrimination against the uv light, which was collinear with the vuv radiation and $>10^4$ times as intense. Care was taken to limit the amount of scattered 193 nm radiation in the interaction chamber as this was the main source of background signal from the Pt p.d. In cases where sum-frequency mixing was employed to generate vuv radiation, an additional precaution was needed. Fre-

quency tripling can occur simultaneously with sum-frequency mixing and therefore both vuv and xuv radiation may be present in the probe beam. Since the detected $H_2$ signal depends only on the vuv light but the photodiode signal responds to both, a LiF window was placed in front of the Pt p.d., acting as a filter which transmits only the vuv photons.

For the measurements of D atom elimination it was necessary to generate Lyman-alpha radiation. This radiation was generated by sum-frequency mixing in a pulsed jet of Kr. This process has been previously reported in a low pressure gas cell.[29] The D atoms were then ionized via (1+1) REMPI in a fashion analogous to the $H_2$ ionization. The detection sensitivity for D atoms was estimated to be $10^4$ atoms/cm$^3$.

The normal ethylene was ultrahigh purity grade ($>99.995\%$) from Matheson. The 1,1-$d_2$ ethylene was obtained from MSD Isotopes and was 98% pure. The $C_2D_4$ was also obtained from MSD and was 99% pure. All gases were used neat and without further purification.

For the determination of the population distributions of $H_2$ products, 800 mbar of $C_2H_4$ was expanded through the 0.5 mm nozzle of a pulsed valve.[30] The pulse duration was 150 $\mu$s. The photolysis laser was timed so as to intersect the molecular beam 80 $\mu$s after the start of the pulse. A 1.02 mm diameter skimmer (Beam Dynamics) was located 1.5 cm from the nozzle separating the source chamber from the differentially pumped main chamber. The distance from the skimmer to the interaction region was 5 cm. The interaction region was located in the extractor of a Wiley–McLaren-type TOF mass spectrometer. The source chamber pressure was $2\times10^{-4}$ Torr and the main chamber pressure was $<2\times10^{-6}$ Torr when the valve was in operation. For the long photolysis/probe time delay studies the skimmer was changed to a low profile 2 mm diameter model, located 2 cm from the nozzle and 4.5 cm from the interaction region. When using the deuterated compounds, the backing pressures were typically around 200 mbar and the molecular beam pulse duration was reduced to 100 $\mu$s (to reduce gas consumption). Although clusters could be detected via single-vuv photon ionization when $C_2H_4$ was seeded in a rare gas carrier, none could be seen in the expansion of neat ethylene when the valve backing pressure was below 1000 mbar.

The molecular beam diameter was calculated to be 5 mm in the interaction region and the probe beam spot size was estimated to be 100–200 $\mu$m. The delay between the photolysis and probe beams was 20 ns for the population scans. The $H_2^+$ signals were normalized to both the vuv dependent signal from the Pt p.d. and to the 193 nm dependent signal from the pyroelectric detector. All acquired signals were processed by boxcar integrators (SRS 250) and averaged slightly (1/3 of the data collection time constant) before being ratioed by analog processors (SRS 225/235). This was done to prevent overloading of the dividing circuitry by the large fluctuations in the vuv intensity. The averaged output from the final analog processor was then recorded by the 699-29 computer (Apple II).

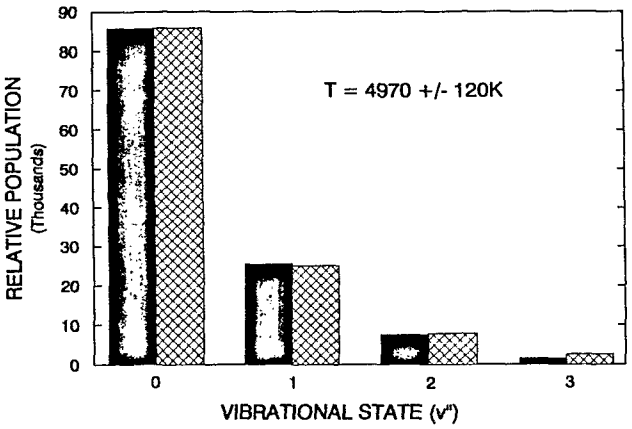


FIG. 5. Distribution of vibrational energy in $H_2$ product from the dissociation of $C_2H_4$ (solid bars). A statistical fit to the distribution ($T=4970\pm120$ K) is also shown (hatched bars).

All data were transferred from the 699-29 to a PC computer for analysis.

## III. RESULTS AND ANALYSIS

### A. Populations

The vibrational distribution of the $H_2$ product from the dissociation of $C_2H_4$ at 193 nm is shown in Fig. 5. The rotational distributions of the same product for the vibrational levels $v''=0$ through $v''=3$ are shown in Fig. 6. Each $H_2$ transition was scanned twice and, whenever possible, $P$, $Q$, and $R$ transitions were used. This provided up to six separate determinations of the population of a given rovibrational state.

The $H_2$ quantum state populations were derived in the following manner. The line shape of each transition was fit by a nonlinear least squares method to the function[31]

$$I \propto \frac{C}{v_D} \times [1+\beta \times P_2(\cos\theta) \times P_2(\chi)], \tag{5}$$

where $v_D$ = maximum Doppler shift, $\beta$=effective anisotropy parameter, $P_2$ = second order Legendre polynomial, $\theta$=angle between the electric field vector of the photolysis laser and the direction of the probe laser (which was 90° in our experiment), $\chi$=Doppler shift/$v_D$, and $C$ is proportional to the line intensity. In our study this function was convoluted with a normalized Gaussian $H_2$ velocity distribution of a variable width. This is justified by the observation of Gaussian-type velocity distributions in the molecular beam photofragment translational spectroscopy experiment reported elsewhere.[14] For overlapping transitions partial fits were done to that part of the line shape that exhibited no interference. Line intensity measurements from these partial fits were used in the population distributions but the Doppler widths and anisotropy parameters were not considered reliable.

An in-depth study of the anisotropy parameters was not undertaken during this experiment. The reasons are twofold. The experimental detection geometry did not lend

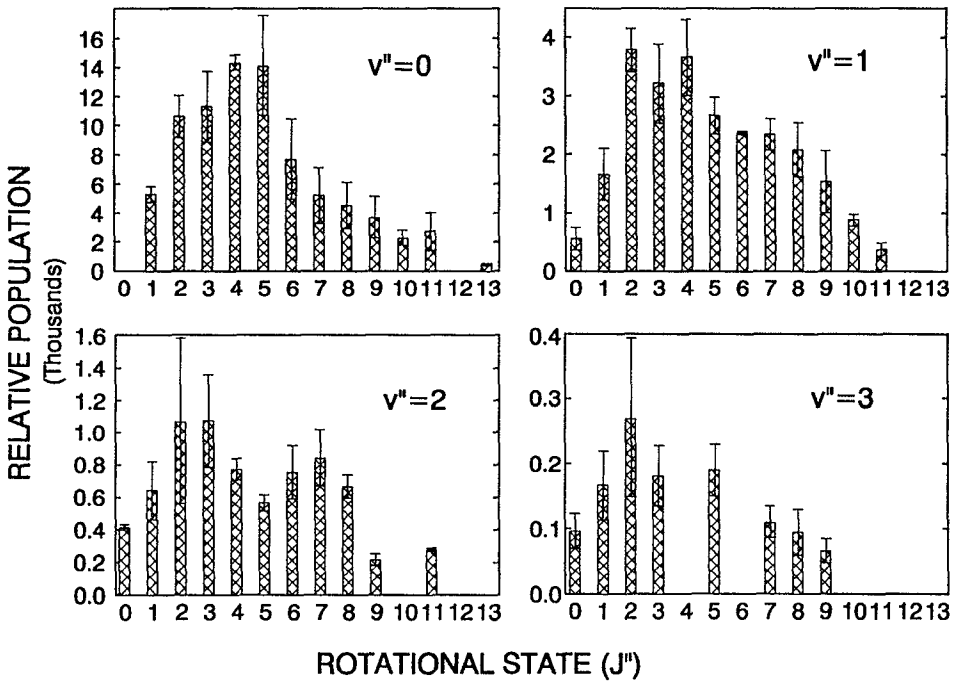


FIG. 6. Distribution of rotational energy in $H_2$ product from the dissociation of $C_2H_4$ for the vibrational levels $v''=0$ to $v''=3$. The various rotational distributions as well as the vibrational distribution (Fig. 3) have the same relative scale. The error bars represent ± one standard deviation of the measurements.

itself to measuring correlations between the electric field vector of the photolysis laser and the product velocity or angular momentum distributions. Furthermore, the observations of other correlations [such as a (**v**, **J**) correlation] would be complicated by the presence of two $H_2$ elimination channels. While nonzero anisotropy parameters were measured ($-0.5<\beta<0.5$), no systematic behavior of the parameters was found.

The relative $H_2$ populations were calculated from the measured line intensities in the manner described previously.[24] When comparing populations for a given $H_2$ quantum state that were measured from different transitions (e.g., *P* branch vs *R* branch), significant discrepancies, due to inaccuracies in the calculated line strength factors, were noted. The large error bars seen for a few of the $H_2$ quantum state populations in Fig. 6 are a result of these discrepancies. Such differences had been seen previously for different $H_2$ transitions when comparing the ratio of calculated $H_2$ emission probabilities to measured values.[32] The difficulty in calculating accurate line strengths arises from perturbation of the energy levels due to rotational coupling between the $B\,^1\Sigma_u^+$ and $C\,^1\Pi_u$ electronic states of $H_2$. Reproduceability for a given transition was very good, attesting to the effectiveness of the normalization techniques used.

There are a number of immediate observations to be made from the distributions shown in Figs. 5 and 6. First, the $H_2$ product is vibrationally very hot and the distribution of energy among the vibrational quantum states appears statistical. This indicates that the H–H distance at the ethylene transition state(s) is elongated with respect to the equilibrium H–H distance of molecular hydrogen. There is also a significant amount of translational and rotational energy released in the dissociation, with $H_2$ observed up to the $J=13$ level (which corresponds to $\approx$30 kcal/mol). This amount of rotational excitation suggests an asymmetric transition state in which the C–H distances are significantly different. In addition, the $H_2$ rotational distributions have unusual shapes, especially for $v''=2$. The nonstatistical distributions, which look somewhat bimodal, could be indicative of two competing $H_2$ elimination channels: namely, 1,1*E* and 1,2*E*. In a later section, we speculate on the nature of the energy release for each of these channels.

The rotational state population distributions of $H_2$ product from 1,1-$d_2$ ethylene were measured in order to help understand the normal ethylene distributions. In previous studies of the photodissociation of deuterated ethylene compounds no isotopic scrambling was observed[1,6,14] indicating that $H_2$ elimination occurs on a time scale that is fast compared to isotopic rearrangement. All $H_2$ product from the photodissociation of $CD_2CH_2$, therefore, is assumed to come from the 1,1*E* channel. These rotational distributions for the vibrational levels $v''=0$ and $v''=1$ are shown in Fig. 7. The error bars for the $v''=0$ levels represent the standard deviations of the various population measurements. A statistical nonlinear least squares fit to each of the vibrational levels[24] is also presented in Fig. 7. The rotational temperatures calculated are 2500±200 K for $v''=0$ and 2000±160 K for $v''=1$. Unfortunately, it proved impossible to obtain a reliable $H_2$ vibrational distribution for this system due to high background contam-

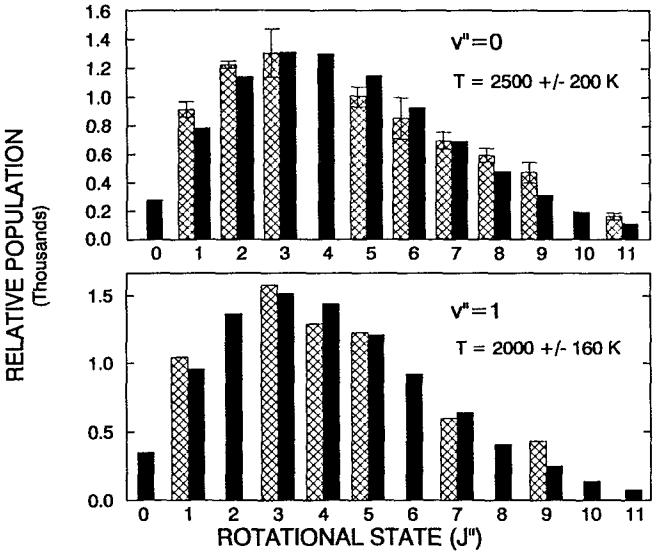


FIG. 7. Distribution of rotational energy in $H_2$ product from the dissociation of 1,1-$d_2$ ethylene for the vibrational levels $v''=0$ and $v''=1$ (hatched bars). Statistical fits to the distributions [$T_R(v''=0) = 2500 \pm 200$ K, $T_R(v''=1) = 2000 \pm 160$ K] are also shown (solid bars). The error bars represent ± one standard deviation of the measurements. The distributions are not to scale to each other.

ination in the mass spectrometer from $D^+$ signal. For similar reasons, we were not able to measure rotational distributions for $v''=2$ and $v''=3$ for this isotopic species.

A statistical fit to the $v''=0$ and $v''=1$ $H_2$ rotational distributions for $C_2H_4$ shown in Fig. 6 yields "temperatures" of $2700\pm250$ K and $2850\pm250$ K, respectively. While for the $v''=0$ level the measured rotational temperature for $H_2$ product from $CD_2CH_2$ is only slightly less than that from $C_2H_4$, the $v''=1$ level shows a significant difference. The measured $H_2$ rotational distributions from the dissociation of 1,1-$d_2$ ethylene, which eliminates $H_2$ only by reaction (3), clearly show that the amount of energy partitioned into $H_2$ rotation for this channel is less than the amount of rotational energy measured in the $H_2$ product from the dissociation of $C_2H_4$. It is important to note that this observation is indicative of the existence of two separate elimination channels. The amount of rotational energy in $H_2$ from the 1,2$E$ channel must be higher than that from the 1,1$E$ channel in order to properly fit the total $H_2$ rotational distribution.

Energetically, one can understand the decrease in rotational energy for higher vibrational levels, especially for 1,1$E$, by considering that for $v''=3$ the $H_2$ vibrational energy is 33.6 kcal/mol. Given the translational energy of $\approx$15 kcal/mol for this level, there is much less energy available for $H_2$ rotation then at the lower vibrational levels. Furthermore, the 1,2$E$ channel has 106 kcal/mol of energy available for products while the 1,1$E$ channel has only 65 kcal/mol available. This makes $>50\%$ more energy available to product from the 1,2$E$ channel. This is one contributing factor to the higher $H_2$ rotational energy for 1,2 elimination.

The calculated transition state[23] for the 1,1 elimination channel (see Fig. 1) is similar to that for $H_2$ elimination from formaldehyde. Rotational energy distributions for $H_2$ from the photodissociation of formaldehyde have been measured at a number of different excitation energies.[33] While the formaldehyde experiments were done at energies much closer to the threshold for dissociation, the total amount of energy available to the $H_2$ product is comparable to that for the 1,1$E$ channel ($\approx$86 kcal/mol for $H_2CO$ and 65 kcal/mol for $C_2H_4$). The rotational distributions measured by Butenhoff *et al.* for $H_2$ elimination from $H_2CO$ were Boltzmann-like with temperatures of 1730 K for the $v''=1$ level and 1240 K for the $v''=3$ level. The amount and distribution of rotational energy imparted to $H_2$ in the two different dissociative processes is comparable, as are the initial geometries.

Parallels can be drawn between the dynamics of the 1,1$E$ channel of $C_2H_4$ and $H_2$ elimination from $H_2CO$. The formaldehyde dissociation has been successfully described by a modified impulsive model[34] with a large impact parameter. In this model, a single impulse between the departing fragments determines the rotational energy for a given impact parameter, direction of impulse, and available energy. The width of the rotational distributions is accounted for by vibrational motion of the parent molecule at the transition state. The $H_2$ rotational energy distributions appear statistical while the corresponding CO distributions are peaked at high J and are nonstatistical in nature. For the case of $H_2$ elimination from ethylene via 193 nm photolysis, the total energy (148 kcal/mol) is much greater than the transition structure energies ($<100$ kcal/mol) and, therefore, we expect that an impulsive model applied to the calculated transition state geometries will not be meaningful. In other words, due to the excess internal energy, the transition structure is severely distorted with respect to the calculated saddle point minimum structure.

Experimental evidence for this point is revealed in the distribution of rotational energy observed for the $H_2$ product in the 1,2$E$ channel. The transition structure in this case (see Fig. 1) was calculated to have equal C–H bond lengths—suggestive of low rotational excitation for the products. However, the large amount of rotational excitation suggests a highly distorted configuration at the transition state much different than the calculated minimum energy structure.

It is possible, with some speculation, to further analyze the $H_2$ distributions from $C_2H_4$. Specifically, we tried to estimate the contributions of 1,1$E$ and 1,2$E$ to the distributions for $H_2(v''=0)$ and $H_2(v''=1)$. This was done in the following manner. The ratio of the total (i.e., not state specified) $H_2$ product from the 1,1 elimination channel [reaction (3)] to the 1,2 elimination channel [reaction (4)] was taken (from previous measurements using deuterated compounds)[1,6,14] as 3:2. However, we could not measure the relative contribution of each elimination channel to a given vibrational level, i.e., we did not have the vibrational population distributions for the two separate channels. In the *ab initio* studies of Yoshimine, discussed above, the H–H distance at the transition state for the 1,1$E$ channel is calculated to be 0.878 Å, while the corresponding distance

for the 1,2$E$ channel is 0.941 Å.[22] We expect that a larger H–H distance at the transition state should correlate with greater vibrational excitation of the $H_2$ product. Using a harmonic approximation for the H–H extension at each transition state relative to a $H_2(v''=0)$ product molecule, we estimate that the vibrational temperature for $H_2$ from the 1,2$E$ channel should be approximately twice that for $H_2$ from the 1,1$E$ channel. With the above assumptions, the percent contribution of the 1,1$E$ channel to the $H_2$ product in the vibrational levels $v''=0$ to $v''=3$ was 67%, 49%, 32%, and 19%, respectively.

For the $v''=0$ and $v''=1$ levels, the rotational temperature of $H_2$ product from 1,1$E$ [reaction (3)] is known from the deuterated ethylene study. The rotational distribution of $H_2$ product from the 1,2$E$ channel for the $v''=0$ and $v''=1$ levels was estimated by making a nonlinear least squared fit to the difference between the total $H_2$ distribution and the fit for 1,1$E$ (as obtained from the dideuteroethylene study). The rotational temperatures obtained in this manner for the 1,2$E$ channel are $3500\pm940$ K for $v''=0$ and $4000\pm800$ K for $v''=1$. It is noteworthy that these temperatures are significantly hotter than for the 1,1$E$ case.

Due to the speculative nature of the above temperatures, one must be cautious when making inferences from the data. The temperatures derived for the 1,2$E$ channel have very large error bars. This might indicate that this channel produces a nonstatistical distribution of rotational energy in the $H_2$ product. Further evidence for this comes from the $v''=2$ level—the level that showed the clearest evidence of bimodality. It is not possible to reasonably fit the $v''=2$ rotational distribution with two Boltzman distributions.

### B. Average translational energy

In the case of concerted decomposition there is a potential energy barrier in the exit valley and a coupling between relative translation of the products and their internal degrees of freedom. This coupling is indicative of a "tight" transition state. In general, for a concerted decomposition, once the reaction proceeds past the critical configuration in the exit channel, the products formed near the top of the potential energy barrier are rapidly repelled from each other with enhanced translational energy. Additionally, translational energy may be gained by initial parent motions along the reaction coordinate and by the coupling of vibrations at the transition state into translation through exit channel interactions. The formation of $H_2$ in the photodissociation of ethylene can be described as proceeding through a tight transition state. For this case, we expect the potential energy release to be the dominant contribution. This has been observed previously for other concerted $H_2$ elimination reactions with large potential energy barriers.[26,33]

The average $H_2$ velocity associated with each quantum state was calculated from the Doppler fits to the individual line shapes by the procedure described above. From these velocities the average $H_2$ translational energy ($E_{tr} = \frac{1}{2}mv^2$) was calculated. A plot of $E_{tr}$ for $H_2$ vs the internal energy of the molecule is shown in Fig. 8 along with a linear least squares fit to the data. Only those transitions which exhibited no interference from other nearby lines were used in this analysis. It is seen that the product translational energies are high (around 20 kcal/mol) and that they decrease slightly with increasing internal energy.

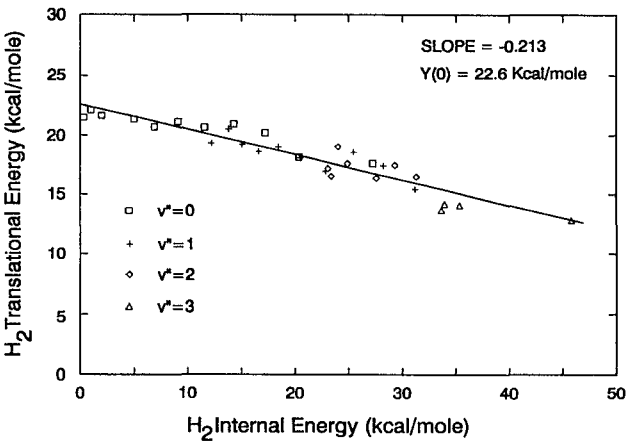


FIG. 8. Plot of translational energy vs internal energy for $H_2$ product from the dissociation of $C_2H_4$. The various vibrational quantum states of the $H_2$ product are indicated.

It would be tempting to treat the elimination of $H_2$ from ethylene as the dissociation of a quasitriatomic molecule (where the hydrocarbon fragment is the third particle) because the calculated transition states[23] reveal that for both channels, the two H atoms recoil from a single carbon atom. In a real triatomic molecule there is a 1:1 trade off between translational and internal energy since the total energy is fixed. In a plot such as that shown in Fig. 8, all data points would lie on a straight line with slope $-1$. The reason why this is not observed in the current experiment is that the major part of the total energy remains within the internal degrees of freedom of the hydrocarbon fragment. In other words, the sum of internal plus translational energies for the $H_2$ fragment need not be constant.

The following simple model explains the observed correlation between the $H_2$ translational and vibrational energies. The model contains two features which are consistent with the observed correlations. At the transition structure, the repulsive energy is expected to depend on the H–H interatomic distance: as the H–H interatomic separation increases, the forming $H_2$ molecule looks less like a closed-shell molecule and, therefore, a weaker repulsion is anticipated. A negative correlation follows from the fact that transition structures with larger H–H interatomic distances are expected to correlate with vibrationally excited $H_2$ product; concomitantly, weaker repulsion is expected to result in lower translational energy.

A second contribution to the observed negative correlation arises from the fact that fairly close to the transition structure (on the exit valley side), the vibration of the $H_2$ product molecules is expected to become adiabatic. A quantum of $H_2$ vibration is very large compared to other

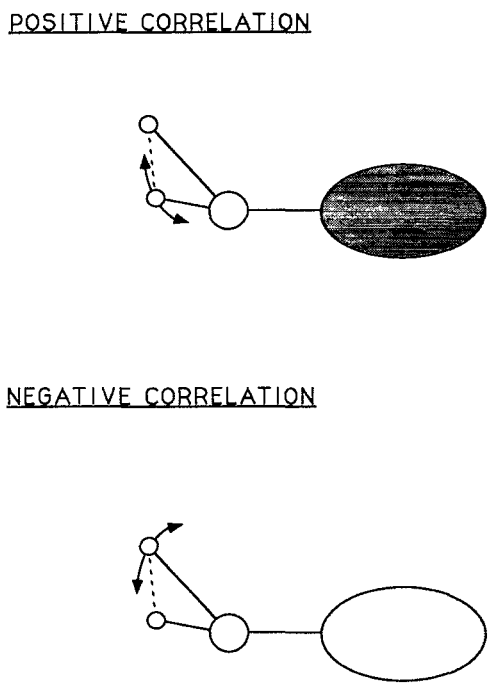


FIG. 9. Cartoon of a three-centered transition state for $H_2$ elimination. (Top) Motion leading to a positive correlation between rotational and translational energy. (Bottom) Motion leading to a negative correlation between rotational and translational energy. The latter case is consistent with our observed correlations.

frequencies in the problem. However, the $H_2$ vibrational frequency is at this point still significantly less than that of a free $H_2$ molecule. Therefore, as the $H_2$ molecule is repelled, some of the repulsive energy release appears as vibrational energy of the $H_2$ molecule and, consequently, less energy will be available for translation. Hence, a negative correlation is expected wherein the $H_2$ translational energy decreases as the vibrational energy increases.

It is also instructive to analyze the amount of $H_2$ translational energy as a function of rotational energy. The distribution of translational energies, shown in Fig. 8, is separated into the various vibrational levels for this purpose. For each vibrational level the translational energy decreases slightly with increasing rotational energy. The behavior for each $v''$ level is somewhat linear. Linear least squares fits to each vibrational level gives slopes of $-0.15$, $-0.19$, $-0.10$, and $-0.10$ for $v''=0$ to $v''=3$, respectively. There is a stronger correlation between vibrational and translational energy than between rotational and translational energy for $H_2$ elimination from ethylene. (There is undoubtedly an effect due to the presence of two $H_2$ elimination channels which complicates any analysis.)

Two transition state models which would lead to a correlation between rotational and translational energy are shown in Fig. 9. These represent limiting cases for the approach to the transition state for $H_2$ elimination from a polyatomic molecule. In this picture, one H atom is much closer to the carbon center than the other. The C,H repulsion for the close H atom is much greater than for the other H atom and therefore makes the dominatant contribution to the translational energy of the $H_2$ product. Due to the excess energy in the reaction, the transition state must be vibrationally excited. The vibrational motions at the transition state can affect the correlations between internal and translational energies of the products.

The first limiting case represents C–H bond rupture where the second H atom interacts only weakly with the carbon atom and the transition state is achieved through motions of the closer H atom. In this case, an increase in repulsive energy will lead to a simultaneous increase in translational energy and rotational energy (since a larger torque is exerted on the $H_2$ species). Therefore, a weak positive correlation would be expected between translational and rotational energy.

The second limiting case represents a situation analogous to a "fly-by pick-off" abstraction reaction. In this case, the transition state is achieved through motions of the farther H atom. As the farther H atom approaches the carbon atom, repulsion increases and enhanced translational energy is expected. However, this same motion also decreases the H–H separation and therefore a smaller torque is exerted on the $H_2$ species, decreasing the rotational excitation. Consequently, a weak negative correlation is expected.

In sum, if the range of motions at the transition state involves the closer of the two H atoms, we expect a weak, positive correlation and if the range of motions involves the farther H atom, then we expect a weak, negative, correlation between $H_2$ translational and rotational energy. Therefore, we suggest that the $H_2$ elimination from ethylene is more consistent with the limiting case shown in Fig. 9(b). It should be pointed out that these models are consistent with the aforementioned discussion of vibrational correlations.

### C. $H_2$ velocity distribution

One of the interests of this experiment was to determine if a difference in translational energy of the $H_2$ product from the two elimination channels of $C_2H_4$ could be measured. Although the distribution of the $H_2$ internal energies suggests a bimodal distribution there is no clear evidence of this in the Doppler profiles themselves, even though the instrument resolution was $<0.1$ cm$^{-1}$. The technique of velocity aligned Doppler spectroscopy (VADS), first noted by Wittig[35] was used to improve the translational energy resolution of the experiment.

In VADS, a long time delay is introduced between the formation of the product and its measurement. In addition, the diameter of the probe and photolysis beams are kept as small as possible. Under these conditions any product with a velocity component directed perpendicular to the probe beam will have moved out of the region that is interrogated by the probe beam during the time between when the photolysis and probe beams are fired. This effectively discriminates against those molecules so the only product molecules that are detected are those directed at or away from the probe beam. The product velocity resolution of the experiment is then greatly enhanced and one can obtain a

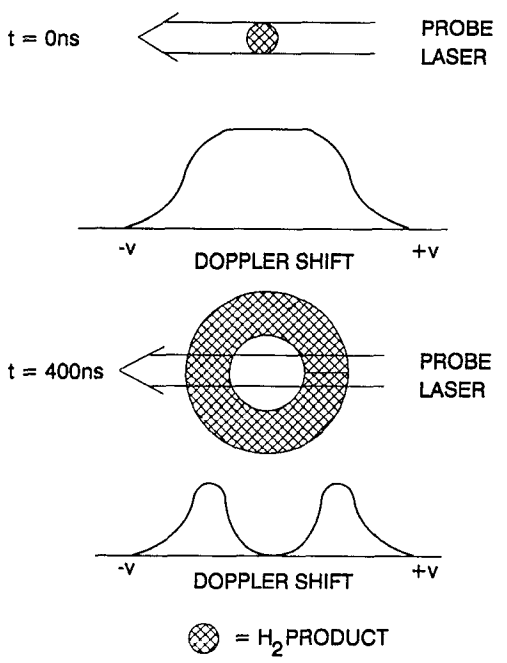


FIG. 10. Pictorial representation of the time delay effect used in velocity aligned Doppler spectroscopy (VADS). Shown are (top) probe beam/$H_2$ product overlap and expected line profile at zero time delay and (bottom) probe beam/$H_2$ product overlap and expected line profile at a long time delay (400 ns). The cross hatched areas represent the spatial distribution of the $H_2$ dissociated from $C_2H_4$.

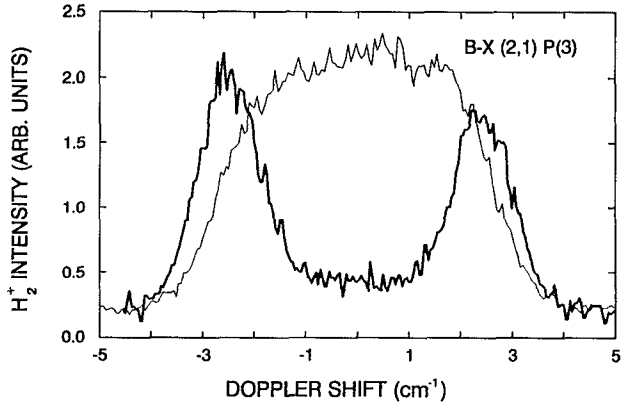


FIG. 11. $H_2$ Doppler profiles measured under VADS conditions for the $v''=1$ level transition $H_2$ $B\leftarrow X$ (2,1) $P(3)$. The VADS profile is shown with a heavy line, while the normal Doppler profile is shown with a light line. The intensity scales are not related.

true speed distribution of the product. A diagram showing this effect is given in Fig. 10.

A number of transitions for the $v''=1$ and $v''=2$ levels were measured under long time delay, or VADS, conditions. Those transitions which exhibited no interference from other lines and had large signals (the signal is significantly reduced under the VADS conditions) produced the best results. The delay between the photolysis and probe lasers needed to observe a VADS profile was dependent on the experimental parameters. The most critical of these was the size of the photolysis beam in the interaction region. The timing varied between 100 ns for a small photolysis beam to 400 ns for a larger beam. The delay was set at the point where no further depletion in signal at the line center could be observed.

For the $v''=1$ level the following $H_2$ transitions were observed under VADS conditions: $B$–$X$ (1,1) $R(1)$, $B$–$X$ (2,1) $P(3)$, and $B$–$X$ (2,1) $R(5)$. For the $v''=2$ VADS profiles were measured for the following transitions: $B$–$X$ (2,2) $R(0)$, $B$–$X$ (2,2) $R(1)$, and $B$–$X$ (3,2) $P(5)$. The measured Doppler profiles under normal and VADS conditions for the $B$–$X$ (2,1) $P(3)$ transition is shown in Fig. 11. It is obvious, from Fig. 11, that the distribution of translational energy in the $H_2$ product is peaked away from zero. This is consistent with molecular beam time-of-flight measurements of this distribution.[18]

The VADS profiles provide information about the distribution of internal energy in the acetylene product. In order to calculate the amount of internal energy in the acetylene molecules that correspond to $H_2$ produced in the six quantum states for which the VADS profiles were obtained, the probe and photolysis lasers were approximated as overlapping lines and a $1/v^2$ weighting was applied to the $H_2^+$ intensities in the VADS profiles. While this is a fairly large approximation, it greatly simplifies the calculation and the average $H_2$ translational energies (measured from the peak of the weighted VADS profile) agree well with those measured from normal Doppler profiles. The calculated acetylene internal energy distributions, therefore, should be reasonable approximations to the true distributions. For each VADS profile the peak acetylene internal energy and the FWHM (full width at half-maximum) of the distribution was calculated according to

$$E^{\text{int}}_{C_2H_2}=E_{\text{avail}}-E^{\text{int}}_{H_2}-E^{\text{tr}}_{H_2}-E^{\text{tr}}_{C_2H_2}.$$

These results are given in Table I. The FWHM's are roughly centered about the peak of the distributions.

The $v''=2$ rotational distribution, shown in Fig. 6, gives the clearest evidence of a bimodal product energy distribution. This led us to undertake a very long time delay VADS study of the $B$–$X$ (2,2) $R(1)$ transition with the hope that the improved velocity resolution (approximately 8%) would allow us to resolve the 1,1$E$ and 1,2$E$ contributions to the VADS line shape. The result of this study is shown in Fig. 12. The Doppler shift extends to almost 4 $cm^{-1}$, corresponding to a $H_2$ translational energy of 46 kcal/mol. Given the $H_2$ internal energy ($v''=2$, $J''=1$; 23 kcal/mol) and the reaction exothermicities from

TABLE I. $C_2H_2$ Internal energy distributions as measured by VADS.

| $H_2$ transition | $V(0)$ ($cm^{-1}$) | Peak $E_{\text{int}}$ (kcal/mol) | $E_{\text{int}}$ FWHM (kcal/mol) |
|---|---|---|---|
| $B$–$X(1,1)R(1)$ | 87 358.22 | 71.5 | 24.5 |
| $B$–$X(2,1)P(3)$ | 88 077.07 | 70.4 | 21.2 |
| $B$–$X(2,1)R(5)$ | 87 709.96 | 69.0 | 19.9 |
| $B$–$X(2,2)R(0)$ | 84 751.31 | 68.5 | 15.5 |
| $B$–$X(2,2)R(1)$ | 84 714.90 | 64.8 | 18.0 |
| $B$–$X(3,2)P(5)$ | 84 729.84 | 61.5 | 17.0 |

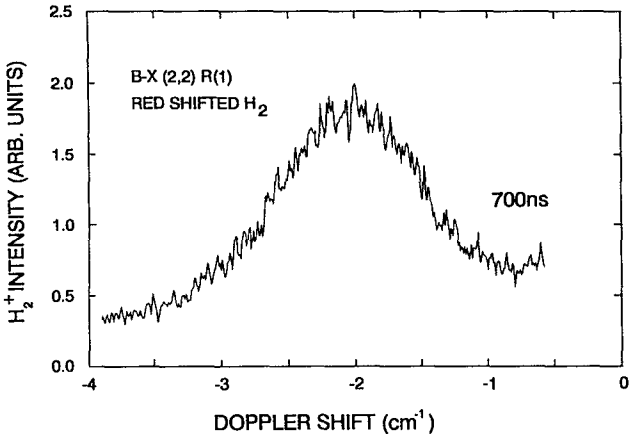


FIG. 12. Red side of VADS profile for $B$–$X$ (2,2) $R(1)$ transition at 700 ns (top trace) time delay. The trace is an average of 10 scans.

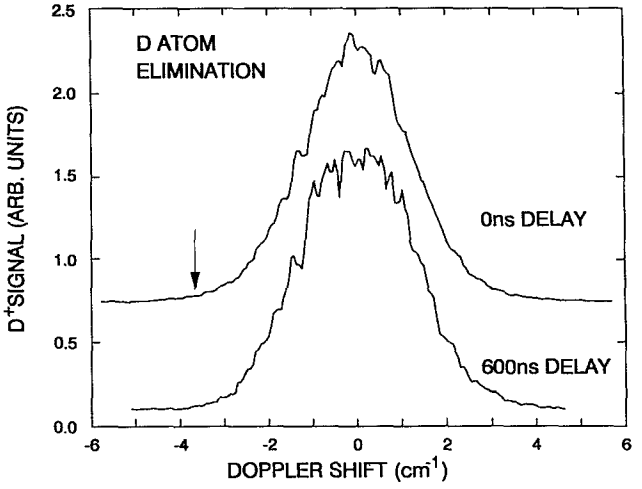


FIG. 13. Scans of the Lyman-alpha transition $\nu_0 = 82\,282.65\ cm^{-1}$) for D atoms eliminated from $C_2D_4$ dissociated at 193 nm under normal delay (top trace) and VADS conditions (bottom trace). The arrow indicates the maximum kinetic energy expected for a single photon event.

Fig. 1, this wing of the Doppler profile must correspond to the 1,2$E$ channel. We might expect to see a slower component, due to 1,1$E$, superimposed on the 1,2$E$ line shape. We do not see clear evidence of this despite the significant differences in exothermicity for the two channels. This is consistent with the majority of the available energy being partitioned to the hydrocarbon fragment, obscuring energetic differences as measured by the $H_2$ Doppler line shape.

One would expect that the Doppler shift observed for $H_2$ dissociating from ethylene through both 1,1 and 1,2 elimination would be larger than that for $H_2$ dissociating from 1,1-$d_2$ ethylene solely from 1,1 elimination. Although no VADS studies were performed for the deuterated species, a comparison of the $H_2$ normal Doppler profiles measured from $C_2H_4$ and $C_2H_2D_2$ reactions for the transitions $C$–$X$ (1,0) $Q(5)$, $C$–$X$ (2,0) $Q(7)$, and $B$–$X$ (2,1) $P(3)$ was made. The $H_2$ translational energies measured from these transitions are given in Table II. As one proceeds to higher energy $H_2$ quantum states, the excess energy for 1,1 elimination becomes considerably less. As a result of this, the $H_2$ translational energy decreases faster for product from the 1,1-$d_2$ ethylene than from $C_2H_4$.

### D. D-atom elimination

In addition to probing the $H_2$ elimination channels in the dissociation of $C_2H_4$, experiments were performed to gain information on the H atom elimination process in this molecule. Due to the presence of large background $H^+$ signals it was necessary to measure D atoms eliminated from $C_2D_4$ photodissociated at 193 nm.

Doppler scans of the D atom Lyman-alpha transition at both short and long (VADS condition) photolysis/probe time delays are shown in Fig. 13. Both scans peak at zero Doppler shift and are fairly narrow in energy as compared with the $H_2$ translational energy. This is consistent with a simple bond rupture in which the translational energy distribution is peaked near zero and with previous measurements of the translational energy distribution in D (and H) atoms eliminated from $C_2D_4$ (and $C_2H_4$).[14,16] The HWHM of the line profiles are 1.43 and 1.57 $cm^{-1}$ for the short and long time delay scans, respectively, corresponding to translational energies of 6.5 and 7.8 kcal/mol, respectively.

An attempt was made to measure the maximum D atom translational energy release in order to estimate the C–D bond strength in $C_2D_4$. D atoms were observed with up to $\approx$70 kcal/mol of translational energy. This would correspond to a C–D bond strength of only $\approx$78 kcal/mol, well below accepted values. Clearly, these fast D atoms cannot be the result of a single photon absorption. Photolysis power dependence studies done on the fast D atom component showed a linear response over an order of magnitude of change in the photolysis energy density. However, this does not rule out a two photon absorption process, as has been previously assumed in other studies of this reaction.[36] If the cross section for absorption of a second photon by a product molecule (such as the vinyl radical) is much greater than that of the first photon this secondary absorption process can be saturated. If this is the case then power dependence studies will produce a linear result.

For the case of ethylene, where the absorption cross section of the product vinyl radical is much greater than that of ethylene,[36,37] a careful photolysis laser power study as a function of D atom Doppler shift did reveal a nonlinear behavior at low intensities, confirming the multiphoton

TABLE II. Translational energy of $H_2$ dissociated from $C_2H_4$ and $CH_2CD_2$ at 193 nm.

| $H_2$ transition | $E_{tr}(H_2)/C_2H_4$ (kcal/mol) | $E_{tr}(H_2)/CH_2CD_2$ (kcal/mol) |
|---|---|---|
| $C$–$X$ (1,0) $Q(5)$ | 21.8 | 22.1 |
| $C$–$X$ (2,0) $Q(7)$ | 21.3 | 19.3 |
| $B$–$X$ (2,1) $P(3)$ | 21.2 | 14 |

nature of the process.[38] This has been observed previously for other concerted $H_2$ elimination reactions with large potential energy barriers.[26,33] This suggests to us that the nascent vinyl radicals produced in the dissociation of ethylene can absorb a second 193 nm photon to produce a second D (or H) atom.

## IV. SUMMARY

The evidence presented in this paper clearly supports the existence of two distinct channels for the elimination of $H_2$ from $C_2H_4$. The existence of these channels, the 1,1 elimination shown in reaction (3) and the 1,2 elimination shown in reaction (4), has been proposed previously and supported by numerous experiments. However, the information presented here provides an insight into differences in the dissociation dynamics of the two processes.

For the 1,1 elimination process, the amount of released energy is limited by the heat of formation of the vinylidene biradical. The average translational energy of $H_2$ from this channel is less than the total average $H_2$ translation energy observed. The amount of rotational energy imparted into the $H_2$ product from this dissociation pathway is also significantly lower than from the other channel. The critical configuration near the transition state for this reaction we suggest to be analogous to that for $H_2$ elimination from formaldehyde.

There is $\approx$50% more energy available to $H_2$ product formed in the 1,2 elimination process. This larger amount of available energy is reflected in the rotational, vibrational, and translational energy of that $H_2$ product. The higher vibrational energy implies a longer H–H distance at the critical configuration of the 1,2 elimination reaction than of the 1,1 elimination reaction. This is consistent with recent *ab initio* calculations of the 1,1*E* and 1,2*E* transition states.[23] The higher rotational energy for the 1,2 elimination is due mostly to the larger kinetic energy release for this channel, despite the fact that the calculated transition state for 1,2*E* is more symmetric than for 1,1*E*. This implies that the critical configuration of the 1,2*E* transition state is significantly distorted from the calculated minimum energy structure by the excess available energy. Furthermore, the poor fit of the 1,2*E* rotational distribution with a rotational temperature suggests that the actual distribution is non-Boltzmann in nature.

Recently, we learned that the barrier in the ground electronic state to 1,2 hydrogen exchange is calculated to be $\approx$75 kcal/mol, corresponding to the heat of formation of ethylidyne.[23] This is barrier is significantly lower than that for either 1,1*E* $H_2$ elimination (at 95 kcal/mol) or 1,2*E* $H_2$ elimination (at 110 kcal/mol). We would expect, therefore, that if the dynamics on the ground state were statistical in nature, then there should be complete isotopic scrambling on the time scale of reaction (i.e., no difference in HD yields between 1,1 dideuteroethylene and 1,2 dideuteroethylene). This is contrary to what is observed.[14] We conclude, therefore, that the elimination reaction exhibits nonstatistical dynamics. This is very interesting: as the molecule has 12 internal degrees of freedom and almost 150 kcal/mol of internal energy, one might expect intramolecular vibrational energy redistribution (IVR) to be extremely rapid and the dynamics, it follows, to be statistical. In the case of 1,1 elimination, excited state ethylene can move directly from the pyramidalized configuration at the crossing of the *N* and *Z* states (see Fig. 2) to the 1,1*E* transition state on the ground state by a simple twisting motion, thus avoiding hydrogen "scrambling." In the case of the 1,2*E* channel, calculations have not yet shown if excited state ethylene can proceed directly to the 1,2*E* transition state on the ground state without going through an ethylidynelike structure (where 1,2 hydrogen exchange may readily occur). However, it is also possible that the system does proceed through such a configuration but traverses quickly as it moves towards the 1,2*E* $H_2$ elimination transition state and the product channel.

Other information presented in this paper helps to further elucidate the dynamics of the dissociation processes. The VADS profiles confirm a concerted elimination mechanism and give an indication as to the distribution of internal energy in the hydrocarbon fragment. The D-atom Doppler profiles confirm that this atomic elimination process occurs on the ground state potential surface. Hopefully, these results will stimulate further experimental and theoretical work, providing a more complete picture of the dissociation dynamics of this important molecule.

## ACKNOWLEDGMENTS

The authors wish to thank Dr. Megumu Yoshimine for communicating to us the results of his calculations prior to publication. A. S. would like to acknowledge NSERC (Canada) for the receipt of a post-doctoral fellowship. This work is supported by the Director, Office of Energy Research, Office of Basic Energy Sciences, Chemical Sciences Division of the U.S. Department of Energy under Contract No. DE-AC03-76SF0098.

[1] P. Ausloos and R. Gorden, Jr., J. Chem. Phys. **36**, 5 (1961).
[2] R. Gorden, Jr. and P. Ausloos, J. Res. Natl. Bur. Std. Sec. A **75**, 141 (1971).
[3] A. B. Callear and R. J. Cvetanović, J. Chem. Phys. **24**, 873 (1955).
[4] R. A. Bach and D. W. L. Griffiths, J. Chem. Phys. **46**, 4839 (1967).
[5] M. C. Sauer, Jr. and L. M. Dorfman, J. Chem. Phys. **35**, 497 (1961).
[6] H. Okabe and J. R. McNesby, J. Chem. Phys. **36**, 601 (1961).
[7] E. Tschuikow-Roux, J. R. McNesby, W. M. Jackson, and J. L. Faris, J. Phys. Chem. **71**, 1531 (1967).
[8] P. Borrel, A Cervenka, and J. W. Turner, J. Chem. Soc. B 12, 2293 (1971).
[9] H. Hara and I. Tanaka, Bull. Chem. Soc. Jpn. **46**, 3012 (1973).
[10] H. Hara and I. Tanaka, Bull. Chem. Soc. Jpn. **47**, 1543 (1974).
[11] A. H. Laufer, J. Photochem. **27**, 267 (1984).
[12] A. Fahr and A. H. Laufer, J. Photochem. **34**, 261 (1986).
[13] K. M. Ervin, S. Gronert, S. E. Barlow, M. K. Gilles, A. G. Harrison, V. M. Bierbaum, C. H. DePuy, W. C. Lineberger, and G. B. Ellison, J. Am. Chem. Soc. aw2, 5750 (1990).
[14] B. Balko, J. Zhang, and Y. T. Lee, J. Chem. Phys. (in press).
[15] R. J. Buenker, V. Bonacic-Koutecky, and L. Pogliani, J. Chem. Phys. **73**, 1836 (1980).
[16] S. Satyapal, G. W. Johnston, R. Bersohn, and I. Oref, J. Chem. Phys. **93**, 6398 (1990).
[17] M. M. Gallo, T. P. Hamilton, and H. F. Schaefer III, J. Am. Chem. Soc. **112**, 8714 (1990).
[18] A. J. Merer and R. S. Mulliken, Chem. Rev. **69**, 639 (1969).
[19] E. M. Evleth and A Sevin, J. Am. Chem. Soc. **103**, 7414 (1981).
[20] J. D. Goddard, Chem. Phys. Lett. **83**, 312 (1981).

[21] G. J. Collin, Adv. Photochem. **14**, 135 (1988).
[22] K. Raghavachari, M. J. Frisch, J. A. Pople, and P. v. R. Schleyer, Chem. Phys. Lett. **85**, 145 (1982).
[23] M. Yoshimine (private communication).
[24] E. F. Cromwell, Ph.D. thesis, University of California, Berkeley (1991).
[25] E. Cromwell, T. Trickl, Y. T. Lee, and A. H. Kung, Rev. Sci. Instrum. **60**, 2888 (1989).
[26] E. F. Cromwell, D.-J. Liu, M. J. J. Vrakking, A. H. Kung, and Y. T. Lee, J. Chem. Phys. **95**, 297 (1991).
[27] A. H. Kung, T. Trickl, N. A. Gershenfeld, and Y. T. Lee, Chem. Phys. Lett. **144**, 427 (1988).
[28] L. Tonkyn and M. G. White, Rev. Sci. Instrum. **60**, 1245 (1989).
[29] R. Hilbig and R. Wallenstein, App. Opt. **21**, 913 (1982).
[30] D. Proch and T. Trickl, Rev. Sci. Instrum. **90** (1989).
[31] R. N. Dixon, J. Chem. Phys. **85**, 1866 (1986).
[32] H. Abgrall, F. Launay, E. Roueff, and J.-Y. Roncin, J. Chem. Phys. **87**, 2036 (1987).
[33] T. J. Butenhoff, K. L. Carleton, and C. B. Moore, J. Chem. Phys. **92**, 377 (1990).
[34] G. E. Busch and K. R. Wilson, J. Chem. Phys. **56**, 3626 (1972).
[35] Z. Xu, B. Koplitz, and C. Wittig, J. Chem. Phys. **87**, 1062 (1987).
[36] H. E. Hunziker, H. Kneppe, A. D. McLean, P. Siegbahn, and H. R. Wendt, Can. J. Chem. **61**, 993 (1983).
[37] A. Fahr and A. Laufer, J. Phys. Chem. **92**, 7229 (1988).
[38] A. Stolow, B. A. Balko, E. F. Cromwell, J.-S. Zhang, and Y. T. Lee, J. Photochem. and Photobiol. **62**, 285 (1992).